

Gamma Ray Spectra from Thermal Neutron Capture on Gadolinium-155 and Natural Gadolinium

Tomoyuki Tanaka¹, Kaito Hagiwara¹, Enrico Gazzola³, Takashi Sudo^{1,10}, Mandeep Singh Reen¹, Ajmi Ali^{1,3,6,*}, Iwa Ou¹, Rohit Dhir^{1,8}, Pretam Kumar Das^{1,9}, Yusuke Koshio¹, Makoto Sakuda^{1,*}, Atsushi Kimura², Shoji Nakamura², Nobuyuki Iwamoto², Hideo Harada², Gianmaria Collazuol³, Sebastian Lorenz⁴, Michael Wurm⁴, William Focillon⁵, Michel Gonin⁵, and Takatomi Yano⁷

¹*Department of Physics, Okayama University, Okayama 700-8530, Japan*

²*Japan Atomic Energy Agency, 2-4 Shirakata Shirane, Tokai, Naka, Ibaraki 319-1195, Japan*

³*University of Padova and INFN, Italy*

⁴*Institut für Physik, Johannes Gutenberg-Universität Mainz, 55128 Mainz, Germany*

⁵*Département de Physique, École Polytechnique, 91128 Palaiseau Cedex, France*

⁶*Department of Physics, Kyoto University, Kyoto 606-8502, Japan*

⁷*Present address: Kamioka Observatory, ICRR, University of Tokyo, Gifu 506-1205, JAPAN*

⁸*Present address: Research Institute & Department of Physics and Nano Technology, SRM University, Kattankulathur-603203, India*

⁹*Present address: Department of Physics, Pabna University of Science & Technology, Pabna-6600, Bangladesh*

¹⁰*Present address: Research Center for Nuclear Physics (RCNP), Osaka University, Osaka 567-0047, Japan*

**E-mail: aliajmi@okayama-u.ac.jp, sakuda-m@okayama-u.ac.jp*

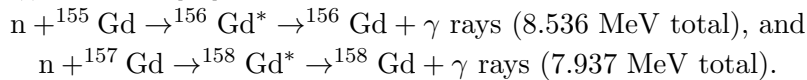
.....
 Natural gadolinium is widely used for its excellent thermal neutron capture cross section, because of its two major isotopes: ¹⁵⁵Gd and ¹⁵⁷Gd. We measured the γ -ray spectra produced from the thermal neutron capture on targets comprising a natural gadolinium film and enriched ¹⁵⁵Gd (in Gd₂O₃ powder) in the energy range from 0.11 MeV to 8.0 MeV, using the ANNRI germanium spectrometer at MLF, J-PARC. The freshly analysed data of the ¹⁵⁵Gd(n, γ) reaction are used to improve our previously developed model (ANNRI-Gd model) for the ¹⁵⁷Gd(n, γ) reaction [14], and its performance confirmed with the independent data from the ^{nat}Gd(n, γ) reaction. This article completes the development of an efficient Monte Carlo model required to simulate and analyse particle interactions involving the thermal neutron captures on gadolinium in any relevant future experiments.

Subject Index D21 Models of nuclear reactions, F22 Neutrinos from supernova and other astronomical objects, C43 Underground experiments, F20 Instrumentation and

technique, H20 Instrumentation for underground experiments, H43 Software architectures

1. Introduction

Gadolinium (Gd) has become an important element of consideration to a number of neutrino experiments for enhanced detection of electron anti-neutrinos ($\bar{\nu}_e$). The presence of Gd boosts the tagging of neutrons in the inverse beta decay reaction (IBD), $\bar{\nu}_e + p \rightarrow e^+ + n$, in organic liquid scintillator and water-Cherenkov detectors. This is primarily due to its large capture cross-section for thermal neutrons and the large energy released by γ rays of $\sim 8\text{MeV}$ for the $\text{Gd}(n, \gamma)$ reactions [11],



The element has already been used as a neutron absorber in scintillator-based detectors [1, 3, 5, 7, 8, 22, 26]. For the upcoming SuperKamiokande-Gd (SK-Gd) phase [29, 32], Gd will be dissolved in a multi-kiloton water-Cherenkov detector.

The application of Gd-loaded detector materials for neutron tagging is foreseen for Direct Dark Matter Search experiments like LZ [4] and XENONnT [23].

Therefore, it is of paramount importance to establish a precise Monte Carlo (MC) model for the γ -ray energy spectrum from the radiative thermal neutron capture on Gd. It is an essential prerequisite for MC studies aiming to evaluate the neutron tagging efficiency in a Gd-loaded detector. Precise modeling is especially important for those detectors which lack hermetic acceptance or/and have a high energy threshold for γ -rays, since some of γ rays emitted in the capture reaction may not be detected.

In most cases, detector materials are doped with the natural Gd (${}^{\text{nat}}\text{Gd}$). Isotopic abundances are listed in Table 1.

Table 1 Relative abundances of gadolinium isotopes in natural gadolinium [28] and their radiative thermal neutron capture cross-sections [24].

Isotope	Abundance[%]	Cross-section[b]
${}^{152}\text{Gd}$	0.200	735
${}^{154}\text{Gd}$	2.18	85
${}^{155}\text{Gd}$	14.80	60900
${}^{156}\text{Gd}$	20.47	1.8
${}^{157}\text{Gd}$	15.65	254000
${}^{158}\text{Gd}$	24.84	2.2
${}^{160}\text{Gd}$	21.86	1.4

The most frequent isotopes, ${}^{155}\text{Gd}$ and ${}^{157}\text{Gd}$, are as well featuring the large cross section of thermal neutron capture. Therefore, the required MC model for ${}^{\text{nat}}\text{Gd}$ requires the modelling of the γ -ray emission from not only ${}^{157}\text{Gd}$ [14] but also ${}^{155}\text{Gd}$.

We measured the γ -ray energy spectrum from the radiative thermal neutron capture on an enriched ${}^{155}\text{Gd}$ sample and a ${}^{\text{nat}}\text{Gd}$ film with the germanium (Ge) spectrometer of the Accurate Neutron-Nucleus Reaction Measurement Instrument (ANNRI) [16, 18–21]. The incident pulsed neutron beam from the Japan Spallation Neutron Source (JSNS) at the Material and Life Science Experimental Facility (MLF) of the Japan Proton Accelerator

Research Complex (J-PARC) [25] and the good γ -ray energy resolution, high statistics and low background makes ANNRI a favorable spectrometer for our intended study [14, 16].

Based on our data and a Geant4 [2, 6] detector simulation of our setup, we develop a model to generate the full γ -ray spectrum from the thermal $^{157,155,\text{nat}}\text{Gd}(n,\gamma)$ reaction. The γ -ray spectrum and its corresponding MC modelling (ANNRI-Gd model) for ^{157}Gd has already been discussed in Ref. [14].

In this report, we present the γ -ray energy spectra from the $^{155}\text{Gd}(n,\gamma)$ and $^{\text{nat}}\text{Gd}(n,\gamma)$ reactions, modify our ANNRI-Gd model with the contribution from ^{155}Gd and present our final MC performance for $^{\text{nat}}\text{Gd}(n,\gamma)$ to be used by any neutrino or other experiment involving the measurement of γ -ray signals from neutron capture on Gd.

2. Experiment and Data Analysis

The 300 kW beam of 3 GeV protons from the JSNS facility in double-bunch mode and a frequency of 25 Hz was incident on a primary target of mercury, producing neutrons. The neutron beam thus produced consist of neutron pulses in double bunch mode, each 100 ns wide, with 600 ns spacing every 40 ms. The ANNRI spectrometer is located 21.5 m away from the neutron beam source. It comprises two germanium cluster detectors with anti-coincidence shields made of bismuth germanium oxide (BGO) and eight co-axial germanium detectors. The target for neutron capture is positioned in line with the beam, at 13.4 cm from each of the two cluster detectors on its either side along the vertical plane. In this report, we used only data taken with the cluster detectors which cover 15% of solid angle. Each cluster consists of seven Ge-crystals in a hexagonal arrangement, details of which can be found in Ref. [14].

The time-of-flight (TOF) information enables a precise selection of neutron events in the energy range from 4 to 100 meV for the analysis. The obtained data covers the energy region of γ rays from 0.11 MeV to about 8 MeV with observed γ -ray multiplicities (M) one to three.

The energies of the emitted γ rays are recorded by each of the crystals. A threshold of 100 keV is set for each of the cluster detectors. For the event classification, we assign a multiplicity value M and a hit value H to each recorded event. We defined the multiplicity M as the combined number of isolated sub-clusters of hit Ge crystals at the upper and the lower clusters. A sub-cluster is formed by the neighboring hit Ge crystals and can be of size ≥ 1 . The hit value H describes the total number of Ge crystals hit in the event. The multiplicity M represents the number of observed γ rays, while the hit value H is a measure of the lateral spread of γ rays. The details of the event class are described in Ref. [14]. (The fraction of the data collected in each event classification are reflected in the barcharts in Fig. A1.)

We used radioactive sources (^{60}Co , ^{137}Cs , and ^{152}Eu) and $^{35}\text{Cl}(n,\gamma)$ to calibrate the detector, and determine the detection efficiency of the spectrometer for γ -rays at energies from 0.3 to 8.5 MeV, as described in details in Ref. [14].

We measured the thermal neutron capture on a gadolinium (Gd_2O_3) target enriched with ^{155}Gd (91.85%) in December 2014 and the natural Gd (99.9% pure metal film) in March 2013. The weights of the targets, i.e., ^{155}Gd and ^{157}Gd powder were 26.4 mg and 28.9 mg respectively, spread across an area of 1cm x 1cm in a teflon envelope. The film of the natural gadolinium target was 5mm x 5mm x 10 μm (and 20 μm) in dimensions. The isotopic composition of our enriched gadolinium sample is given in Table 2.

Table 2 Isotopic compositions of the Gd_2O_3 targets [17].

Isotope:	^{152}Gd	^{154}Gd	^{155}Gd	^{156}Gd	^{157}Gd	^{158}Gd	^{160}Gd
$^{155}\text{Gd}_2\text{O}_3$	<0.02	0.5	91.9(± 0.3)	5.87	0.81	0.65	0.27
$^{157}\text{Gd}_2\text{O}_3$	<0.01	0.05	0.3	1.63	88.4(± 0.2)	9.02	0.6

In 2014, the beam pipe included an additional layer of LiF (~ 1 cm thickness) to reduce the γ rays from neutron capture on the aluminium of the beam pipe. Therefore, the data-taking with $^{\text{nat}}\text{Gd}$ was subject to more background events (without the LiF layer) than that of $^{155,157}\text{Gd}$. The background γ -ray energy spectra which were observed by one of the crystals (C6) for M1H1 events (1γ and 1 hit) with the empty target holder at two different periods in the neutron beam are shown in Fig. 1. The γ -ray energy spectra for M1H1 events with the three target materials, ^{155}Gd , ^{157}Gd (2014) and $^{\text{nat}}\text{Gd}$ (2013) are also shown in Fig. 1. The histograms shown are normalized with reference to the live time of ^{155}Gd data set. The differences in the observed count rates are due to the differences in the target masses (\times cross section) used for the three measurements. The background is accordingly subtracted for each data set and the resulting energy spectra for the three targets are shown in Fig. 2.

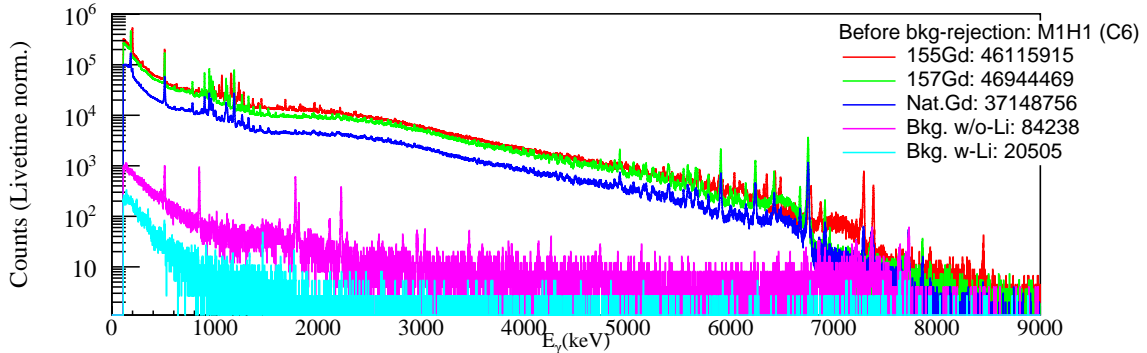


Fig. 1 Energy spectra for M1H1 (1γ and 1 hit) events obtained with neutron beam on the targets ^{155}Gd , ^{157}Gd and natural gadolinium, and the blank target holder as recorded in 2013 (w/o LiF) and 2014 (with LiF). The numbers show the data statistics in each case.

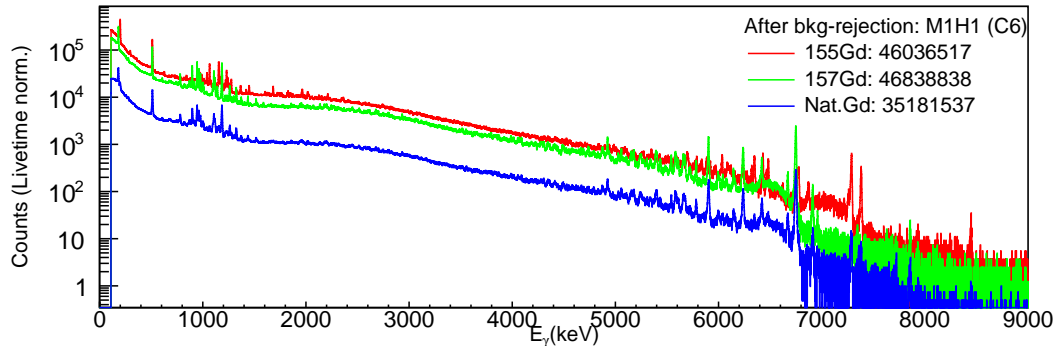


Fig. 2 Energy spectra for M1H1 events obtained with neutron beam on the targets ^{155}Gd , ^{157}Gd and natural gadolinium, after subtracting the background. The numbers show the data statistics in each case.

The γ -ray energy spectrum from neutron capture on natural gadolinium is dominated by that from its two main isotopes, ^{155}Gd and ^{157}Gd , with fractions of 18.5% and 81.5%, respectively. The contributions of other isotopes are negligible.

The spectra taken separately for the pure ^{155}Gd and ^{157}Gd samples must be consistent with that of the ^{nat}Gd film, when they are combined in the corresponding proportions. This was checked and confirmed in Fig. 3, where excellent agreement is found between the two spectra (red and black).

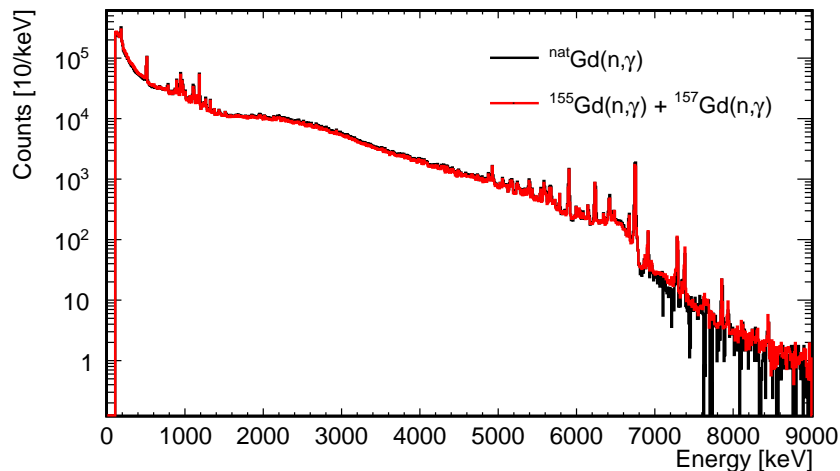


Fig. 3 Comparison of the combined energy spectra of ^{155}Gd and ^{157}Gd (red) with that of the natural gadolinium (black).

3. Update of ANNRI-Gd Model

The MC model for ^{157}Gd has been already described in Ref. [14]. We now develop the same for ^{155}Gd , following the same strategy [14, 15] of a separate treatment of the discrete and the continuum part of the spectrum.

For the thermal neutron capture on ^{155}Gd in an s-wave, the resonance state is 8.536 MeV ($J^\pi = 2^-$) of ^{156}Gd . The resonance energy for the neutron is 26.8 ± 0.2 meV and the radiative width is 108 ± 1 meV [24]. We identified and measured the photo peak intensities of 12 discrete γ rays for $^{155}\text{Gd}(n, \gamma)$ above 5 MeV as listed in Table 3. The single and double escape peaks were excluded before analysing these peaks. The direct transition of the resonance state ($J^\pi = 2^-$) to the ground state ($J^\pi = 0^+$) is largely suppressed compared to the transition from 8.536 MeV ($J^\pi = 2^-$) to 0.089 MeV ($J^\pi = 2^+$), emitting a 8.448-MeV γ ray. The tabulated values of the energies are taken from Ref. [27]. In case of overlapping peaks in our data spectrum, we mention the means of the primary γ -ray energies with their combined intensities. The discrete γ -ray emissions above 5 MeV are expected to arise mostly from the first transition and are hence referred to as ‘primary’ γ rays. By tagging the events with each of these primary γ rays, we obtained the intensities of the secondary γ rays. We found them in fair agreement with the values from ENSDF [27], as displayed in Fig. 4. Details of the comparison methods are described in Ref. [14]. The relative intensities of these discrete peaks add up to $2.78 \pm 0.02\%$ of the data spectrum.

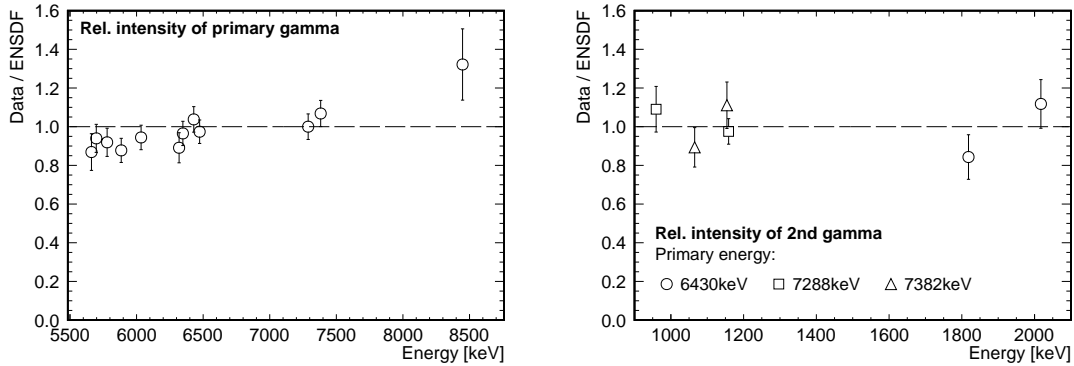


Fig. 4 Relative intensity of the primary peaks (left) and the secondary γ rays (right) compared with the values from ENSDF [27].

For the modelling of the continuum part, we compute the probability $P(E_a, E_b)$ for E1 transitions with $E_\gamma = E_a - E_b$ in terms of transmission coefficient $T_{E1}(E_\gamma)$ and the number of levels $\rho(E_b)\delta E_b$ as

$$P(E_a, E_b) \approx \frac{dP}{dE}(E_a, E_b) \delta E = \frac{\rho(E_b)T_{E1}(E_\gamma)}{\int_0^{E_a} \rho(E'_b)T_{E1}(E'_\gamma) dE'_b} \delta E, \quad E'_\gamma = E_a - E'_b, \quad (1)$$

where δE is a finite energy step in our computations. $T_{E1}(E_\gamma)$ refers to the E1 Photon Strength Functions (PSF) depending on cross section (σ_i), the width (Γ_i) and energy (E_i) of the resonances. It is written as

$$T_{E1}(E_\gamma) = 2\pi E_\gamma^3 \frac{1}{3\pi(\hbar c)^2} \sum_{i=1}^4 \frac{\sigma_i E_\gamma \Gamma_i^2}{(E_\gamma^2 - E_i^2)^2 + E_\gamma^2 \Gamma_i^2}, \quad (2)$$

Table 3 List of the 12 discrete peaks from primary γ rays we identified in our data. The stated energies are taken from Ref. [27], rounded to nearest keV. In four cases the table lists the unweighted mean energy of known peaks that overlap in our data: (i) 6474 keV combining 6482 keV and 6466 keV, (ii) 6348 keV combining 6349 keV and 6345 keV, (iii) 5885 keV combining 5889 keV and 5884 keV, as well as (iv) 5779 keV combining 5774 keV and 5786 keV.

	γ -ray energy [keV]			Intensity % [10^{-2}]
	Primary	Secondary		
1	8448	–	–	1.8 ± 0.2
2	7382	1154	–	12.7 ± 1.4
		1065	–	10.6 ± 1.2
3	7288	1158	–	34.8 ± 2.4
		959	199	10.5 ± 1.1
4	6474	1964	–	35.2 ± 0.7
5	6430	2017	–	20.7 ± 2.2
		1818	199	11.7 ± 1.5
6	6348	2188	–	12.1 ± 1.7
		2097	199	9.8 ± 1.6
		1036	1154	4.6 ± 0.8
			1065	3.8 ± 0.7
7	6319	2127	–	9.4 ± 0.5
8	6034	2412	–	14.0 ± 1.7
		2213	199	6.4 ± 1.0
9	5885	2563	–	9.0 ± 2.1
		2364	199	8.4 ± 2.1
10	5779	2672	–	18.8 ± 0.8
11	5698	2749	–	28.6 ± 0.8
12	5661	2786	–	15.4 ± 0.7

where values of E_i , σ_i and width Γ_i are mentioned in Table 4¹ and $\rho(E_b)$ is the nuclear level density (NLD).

The corresponding NLD $\rho(E_b)$ and the PSFs used for ^{156}Gd are shown in Fig. 5 (left and right respectively).

4. Final model performance

We first generate the continuum part of the γ -ray spectrum in ^{156}Gd according to Eq. (1). The result is shown in Fig. 6. We then generate the discrete part according to the relative intensities listed in Table 2 and then compare these two parts with the observed spectrum. We determine the fraction of the discrete part in the total number of events to be $2.78 \pm 0.02\%$ of the data above 0.11 MeV. The remaining dominant contribution of $97.22 \pm 0.02\%$ comes

¹The M1 and E2 resonances are not considered here for the same reasons stated in our previous work [14].

Table 4 Parameter values for the PSF of the ^{156}Gd nucleus [30]. We use the E1 resonances for our model.

Index i	Cross-section σ_i [mb]	Energy E_i [MeV]	Width Γ_i [MeV]
(E1) 1	242	15.2	3.6
(E1) 2	180	11.2	2.6
(E1) 3	2.0	6.0	2.0
(E1) 4	0.4	3.0	1.0
(M1) 5	2.03	7.62	4.0
(E2) 6	3.69	11.7	4.24

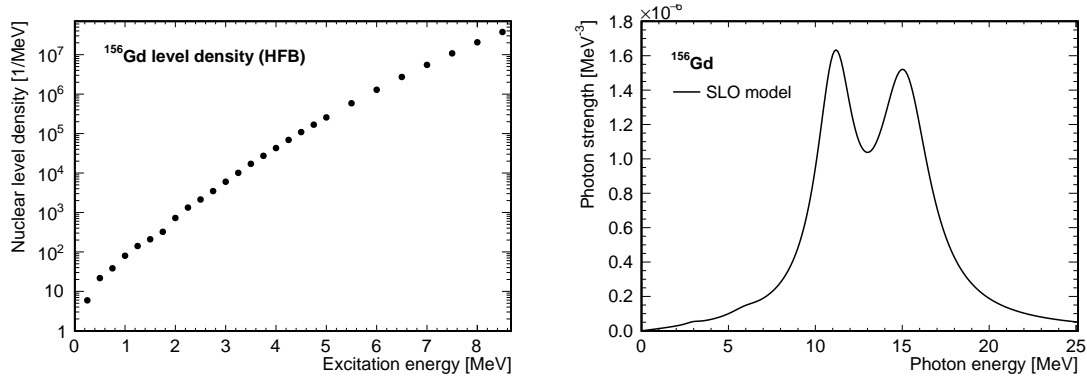


Fig. 5 Left: Tabulated values [9, 10] for the NLD of ^{156}Gd from computations based on the HFB method [12, 13]. Right: The E1 PSFs for ^{156}Gd , given as a function of the γ -ray energy, used in the SLO approach.

from the continuum part of the energy levels in ^{156}Gd . The continuum and the discrete components generated by our MC model are shown separately here for ^{155}Gd , along with the data in Fig. 7. They are added in the corresponding fractions in Fig. 8-left. The data spectrum matches well with our MC spectrum.

The MC generated spectrum for $^{\text{nat}}\text{Gd}(n, \gamma)$ should naturally comprise the spectrum for $^{155}\text{Gd}(n, \gamma)$ and $^{157}\text{Gd}(n, \gamma)$, as is obvious with the data spectra in Fig. 3. So, the spectrum for $^{\text{nat}}\text{Gd}(n, \gamma)$ is obtained by adding the MC spectra generated for $^{155}\text{Gd}(n, \gamma)$ and $^{157}\text{Gd}(n, \gamma)$ in the required ratio of their relative cross-section and abundance, as is shown in Fig. 8-right.

The spectra shown above are single energy spectra (M1H1), which constitute the most dominant ($\sim 70\%$) fraction of the data. In fact, good agreement is found between all the MC generated spectra and the subsamples of data for different observed multiplicities M . Exemplarily, the M2H2 and M3H3 spectra are shown in appendix A.

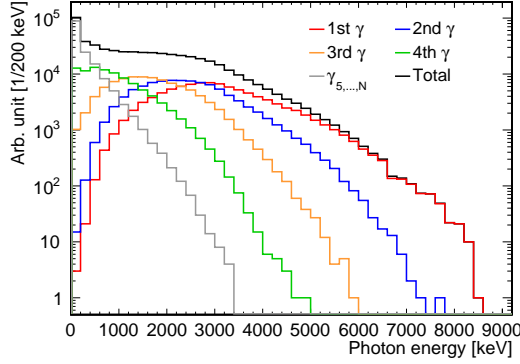


Fig. 6 Continuum component (black) according to our model for the γ -ray energy spectrum from the $^{155}\text{Gd}(n, \gamma)$ reaction and its composition in terms of contributions from the first (red), second (blue), third (orange), fourth (green) γ ray and other γ rays (gray).

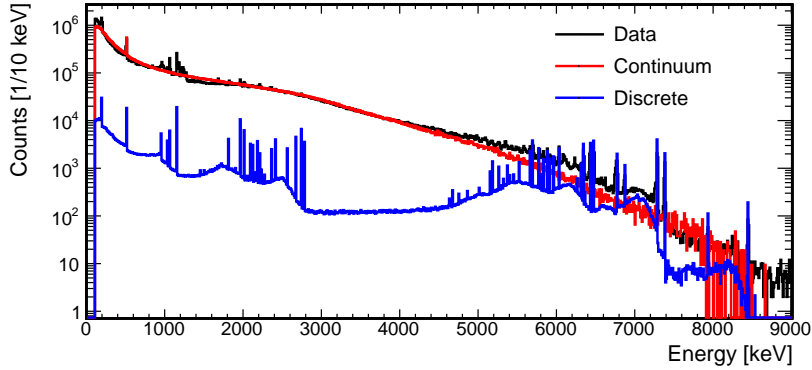


Fig. 7 The continuum and the discrete components of the spectrum generated by the MC shown separately along with the data spectrum.

5. Conclusion

The γ -ray spectra generated by our ANNRI-Gd model agree not only with the individual ^{155}Gd and ^{157}Gd data set, but also with $^{\text{nat}}\text{Gd}$ data set, which are entirely independent². We show the ratio of data/MC in bins of 200 keV for ^{155}Gd , ^{157}Gd , and $^{\text{nat}}\text{Gd}$ in Fig. 9, for the single γ -ray $M = 1$ events as an approximate representation of the goodness of our model. The same ratios for event classes $M = 2$ and $M = 3$ are shown in Figs. A4, respectively. They are all in good agreement at a similar level to those published for the $^{157}\text{Gd}(n, \gamma)$ reaction [14]. With this article, we have completed a consistent model (ANNRI-Gd Model) to generate the gross spectrum for the thermal ^{155}Gd , ^{157}Gd and $^{\text{nat}}\text{Gd}(n, \gamma)$ reaction. In comparison, the more sophisticated model [31] tries to include a small contribution of M1 (scissors mode) or E2 resonance around 3 MeV to PSF in order to explain the energy spectra

² The data of ^{155}Gd and ^{157}Gd were used to tune the discrete part of our MC model, while the $^{\text{nat}}\text{Gd}$ data was untouched during the building of our MC.

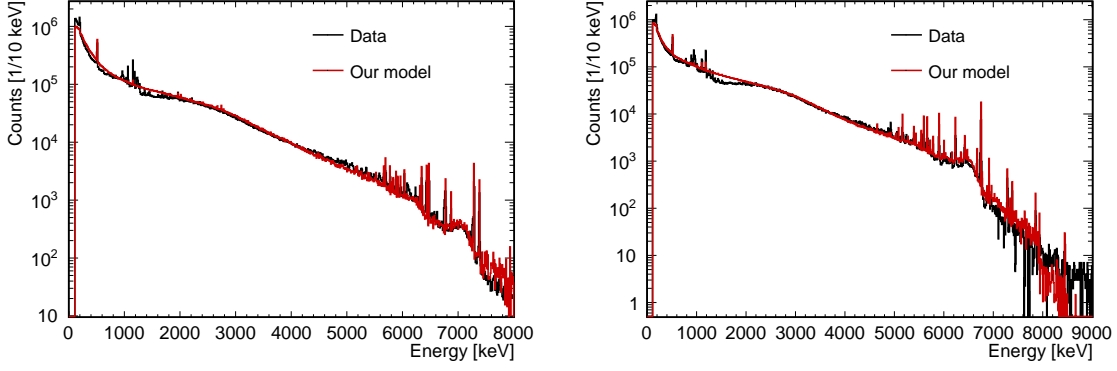


Fig. 8 Single Energy spectrum (M1H1) generated by our model compared with the data for ^{155}Gd on left, and $^{\text{nat}}\text{Gd}$ on right.

in the sample of 2 cascade γ rays. To further refine the present modeling, we intend to work on a sample of 2 γ rays including strong discrete cascade transitions. We note that those samples constitute at most a few % or less of the total number of capture events.

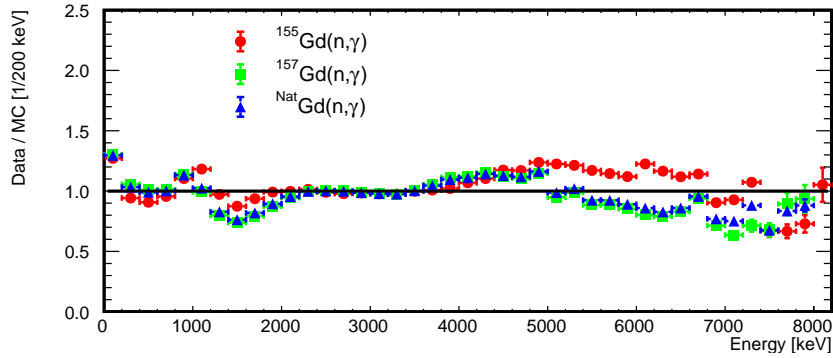


Fig. 9 Ratio of data by MC for the single γ events (M1H1 + M1H2) obtained for $^{157}\text{Gd}(n,\gamma)$, $^{155}\text{Gd}(n,\gamma)$ and $^{\text{nat}}\text{Gd}(n,\gamma)$ cases.

Acknowledgement

This work is supported by the JSPS Grant-in-Aid for Scientific Research on Innovative Areas (Research in a proposed research area) No. 26104006 and No. 15K21747. It benefited from the use of the neutron beam of the JSNS and the ANNRI detector at the Material and Life Science Experimental Facility of the Japan Proton Accelerator Research Complex.

Appendices

A. Double/Triple γ -Ray Spectra

Apart from the single γ -ray events ($M=1$), $M=2$ and $M=3$ γ -ray events are also observed. The M1H1 sample is the most dominant one, followed by the M1H2 sample. Our model agrees in both cases. The event statistics are shown in Fig. A1. The corresponding spectra for M2H2 and M3H3 generated by our model also agree well with the $^{155}\text{Gd}(n,\gamma)$ and the

$^{nat}\text{Gd}(n,\gamma)$ data, as shown in Fig. A2 and A3 respectively. The ratio of data/MC is also shown in Fig. A4.

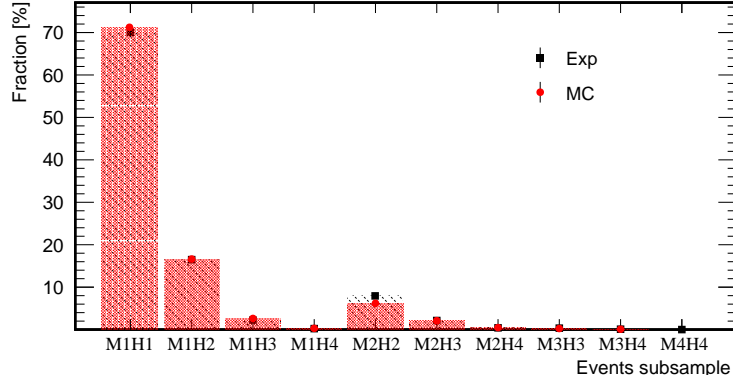


Fig. A1 Event statistics in fraction (%) in the Data and MC under the different event classification.

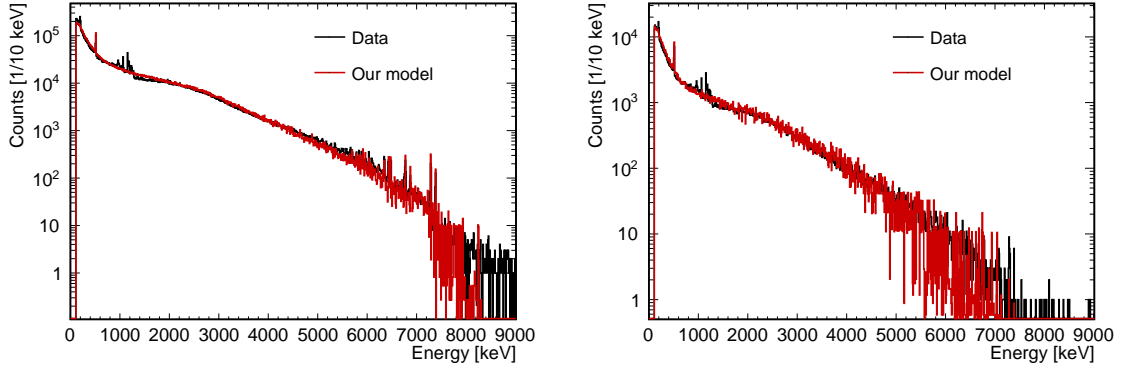


Fig. A2 The $^{155}\text{Gd}(n,\gamma)$ spectra for M2H2(left) and M3H3(right) classified events from data and our model MC.

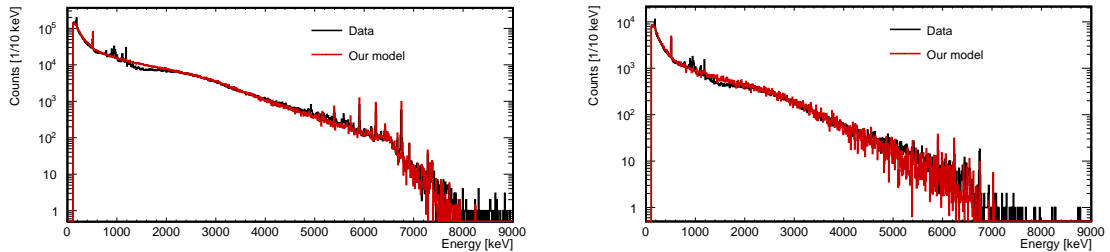


Fig. A3 The $^{nat}\text{Gd}(n,\gamma)$ spectra for M2H2(left) and M3H3(right) classified events from data and our model MC.

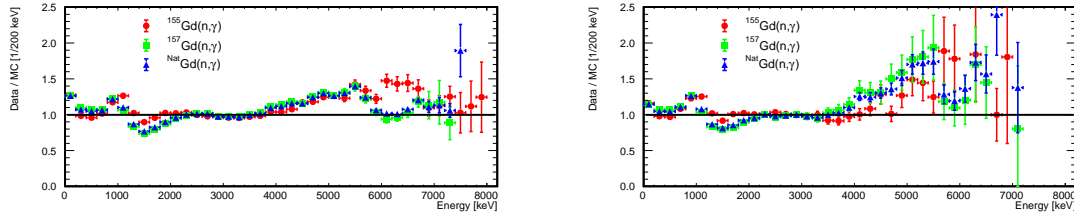


Fig. A4 Ratio: Ratio of data/MC of the single γ -ray events, M2H2 (left) and M3H3 (right) obtained for $^{157}\text{Gd}(n,\gamma)$, $^{155}\text{Gd}(n,\gamma)$ and $^{\text{nat}}\text{Gd}(n,\gamma)$ cases.

References

- [1] ABE, Y. ET AL. [DOUBLE CHOOZ COLLABORATION] (2012) Indication of Reactor $\bar{\nu}_e$ Disappearance in the Double Chooz Experiment. *Phys. Rev. Lett.*, **108**, 131801.
- [2] AGOSTINELLI, S. ET AL. [GEANT4 COLLABORATION] (2003) Geant4—a simulation toolkit. *Nucl. Instrum. Meth.*, **A506**, 250–303.
- [3] AHN, J. K. ET AL. [RENO COLLABORATION] (2012) Observation of Reactor Electron Antineutrinos Disappearance in the RENO Experiment. *Phys. Rev. Lett.*, **108**, 191802.
- [4] AKERIB, D. S. *et al.* (2019) Measurement of the Gamma Ray Background in the Davis Cavern at the Sanford Underground Research Facility.
- [5] ALEKSEEV, H. ET AL. (2018) Search for sterile neutrinos at the DANSS experiment.
- [6] ALLISON, J. ET AL. [GEANT4 COLLABORATION] (2006) Geant4 developments and applications. *IEEE Trans. Nucl. Science*, **53**, 270–278.
- [7] ALMAZAN, H. ET AL. (2018) Sterile Neutrino Constraints from the STEREO Experiment with 66 Days of Reactor-On Data. *Phys. Rev. Lett.*, **121**, 161801.
- [8] AN, F. P. ET AL. [DAYA BAY COLLABORATION] (2012) Observation of Electron-Antineutrino Disappearance at Daya Bay. *Phys. Rev. Lett.*, **108**, 171803.
- [9] CAPOTE, R. ET AL. (2009a) RIPL – Reference Input Parameter Library for Calculation of Nuclear Reactions and Nuclear Data Evaluations. *Nucl. Data Sheets*, **110**, 3107–3214.
- [10] CAPOTE, R. ET AL. (2009b) RIPL3 – Reference Input Parameter Library for Calculation of Nuclear Reactions and Nuclear Data Evaluations. *Nucl. Data Sheets*, **110**, 3107–3214.
- [11] FIRESTONE, R., D. CHOI, H., M. LINDSTROM, R., L. MOLNAR, G., MUGHABGHAB, S., PAVIOTTI-CORCUERA, R., REVAY, Z., TRKOV, A., M. ZHOU, C. & ZERKIN, V. (2007) Database of prompt gamma rays from slow neutron capture for elemental analysis.
- [12] GORELY, S., SAMYN, M. & PEARSON, J. M. (2007) Further explorations of Skyrme-Hartree-Fock-Bogoliubov mass formulas. VII. Simultaneous fits to masses and fission barriers. *Phys. Rev. C*, **75**, 064312.
- [13] GORELY, S., HILAIRE, S. & KONING, A. J. (2008) Improved microscopic nuclear level densities within the Hartree-Fock-Bogoliubov plus combinatorial method. *Phys. Rev. C*, **78**, 064307.
- [14] HAGIWARA, K. ET AL. (2019) Gamma Ray Spectrum from Thermal Neutron Capture on Gadolinium-157. *PTEP*, **2019**, 023D01. http://www.physics.okayama-u.ac.jp/~sakuda/ANNRI-Gd_ver1.html.
- [15] HORTON-SMITH, G. ET AL. (2005) GLG4sim, Generic liquid-scintillator anti-neutrino detector Geant4 simulation. <https://www.phys.ksu.edu/personal/gahs/GLG4sim/>.
- [16] IGASHIRA, M., KIYANAGI, Y. & OSHIMA, M. (2009) Nuclear data study at J-PARC BL04. *Nucl. Instrum. Meth.*, **A600**, 332–334.
- [17] ISOFLEX USA (2014) Certificate of analysis.
- [18] KIMURA, A. ET AL. (2012) Neutron-capture cross-sections of ^{244}Cm and ^{246}Cm measured with an array of large germanium detectors in the ANNRI at J-PARC/MLF. *J. Nucl. Sci. Technol.*, **49**, 708–724.
- [19] KIN, T. ET AL. (2011) The “ 4π Ge Spectrometer” for Measurements of Neutron Capture Cross Sections by the TOF Method at the J-PARC/MLF/ANNRI. *J. Korean Phys. Soc.*, **59**, 1769–1772.
- [20] KINO, K. ET AL. (2011) Measurement of energy spectra and spatial distributions of neutron beams provided by the ANNRI beamline for capture cross-section measurements at the J-PARC/MLF. *Nucl. Instrum. Meth.*, **A626**, 58–66.
- [21] KINO, K. ET AL. (2014) Energy resolution of pulsed neutron beam provided by the ANNRI beamline at the J-PARC/MLF. *Nucl. Instrum. Meth.*, **A736**, 66–74.
- [22] KO, Y. J. ET AL. (2017) Sterile Neutrino Search at the NEOS Experiment. *Phys. Rev. Lett.*, **118**,

-
- 121802.
- [23] MORIYAMA, S. (2019) Direct Dark Matter Search with XENONnT. *International symposium on Revealing the history of the Universe with underground particle and nuclear research, March 7-9, 2019, Sendai.*
 - [24] MUGHABGHAB, S. F. (2006) *Atlas of Neutron Resonances, Fifth Edition: Resonance Parameters and Thermal Cross Sections. Z=1-100.* Elsevier Science.
 - [25] NAGAMIYA, S. (2012) Introduction to J-PARC. *Prog. Theor. Exp. Phys.*, **2012**, 02B001.
 - [26] OGURI, S., KURODA, Y., KATO, Y., NAKATA, R., INOUE, Y., ITO, C. & MINOWA, M. (2014) Reactor antineutrino monitoring with a plastic scintillator array as a new safeguards method. *Nucl. Instrum. Meth.*, **A757**, 33–39.
 - [27] REICH, C. W. (2012) Nuclear Data Sheets for A = 156. *Nucl. Data Sheets*, **113**, 2537–2840.
 - [28] ROSMAN, K. J. R. & TAYLOR, P. D. P. (1998) Isotopic compositions of the elements 1997 (Technical Report). *Pure Appl. Chem.*, **70**, 217–235.
 - [29] SEKIYA, HIROYUKI FOR THE [SUPER-KAMIOKANDE COLLABORATION] (2016) The Super-Kamiokande Gadolinium Project. *PoS, ICHEP2016*, 982.
 - [30] SHIBATA, K., IWAMOTO, O., NAKAGAWA, T., IWAMOTO, N., ICHIHARA, A., KUNIEDA, S., CHIBA, S., FURUTAKA, K., OTUKA, N., OHSAWA, T., MURATA, T., MATSUNOBU, H., ZUKERAN, A., KAMADA, S. & KATAKURA, J.-I. (2011) JENDL-4.0: A New Library for Nuclear Science and Engineering. *Journal of Nuclear Science and Technology*, **48**, 1–30.
 - [31] VALENTA, S., BEČVÁŘ, F., KROLL, J., KRTIČKA, M. & TOMANĎL, I. (2015) Two-step γ cascades following thermal neutron capture in $^{155,157}\text{Gd}$. *Phys. Rev. C*, **92**, 064321.
 - [32] WATANABE, H. ET AL. [SUPER-KAMIOKANDE COLLABORATION] (2009) First study of neutron tagging with a water Cherenkov detector. *Astropart. Phys.*, **31**, 320–328.